Negative Linear Compressibility in $[NH_3NH_2]Co(HCOO)_3$ and its Structural Origin Revealed from First-principles

Partha Sarathi Ghosh*,† and Inna Ponomareva*,†

†*Department of Physics, University of South Florida, Tampa, Florida 33620, USA*

‡*Glass & Advanced Materials Division, Bhabha Atomic Research Centre, Mumbai 400 085, India*

E-mail: psghosh@mail.usf.edu; iponomar@usf.edu

Abstract

First-principles density functional theory computations are used to predict negative linear compressibility in hybrid organic-inorganic perovskite $[NH_2NH_3][Co(HCOO)_3]$. Negative compressibility is a rare exotic response of a material to pressure associated with expansion along one or two lateral directions. Detailed structural analysis revealed that $[NH_2NH_3][Co(HCOO)_3]$ responds to pressure through tilting of its relatively rigid units, CoO_6 polyhedra and $(HCOO)^{-1}$ ligand chain. The $(HCOO)^{-1}$ units form "wine-rack" geometry which is well described with "strut-hinge" model. Within the model, the struts are formed by the rigid units, while hinges are their relatively flexible interconnects. Under pressure the hinge angle increases which leads to the expansion along the direction subtended by the angle. Interestingly, at zero pressure the linear compressibilities in $[NH_2NH_3][Co(HCOO)_3]$ are all positive. As pressure increases the lowest linear compressibility value turns negative and increases in magnitude. Comparison with literature suggests that such a trend is likely to be common to this family of materials. Mechanical properties of $[NH_2NH_3][Co(HCOO)_3]$ are highly anisotropic.

While most materials reduce volume and unit cell dimensions under isotropic pressure, P, a special class of materials counter intuitively expands one or more unit cell dimensions in the process of densification. In this unique mechanical effect, linear, L, compressibilities, $-\frac{1}{L}(\frac{dL}{dP})_T$, or/and area, A, compressibilities, $-\frac{1}{A}(\frac{dA}{dP})_T$, become negative.[1,2] Negative linear compressibility (NLC), a remarkably rare phenomenon, has many potential applications in high pressure conditions, *e.g.*, development of artificial muscles, highly sensitive pressure detectors, robust shock absorbing materials, 'smart' body armor, optical-telecommunication devices functional at deep sea atmosphere, and amplification of piezoelectric response for next generation sensors and actuators.[1,3]

Cairns *et al.*[2] classified NLC materials in four distinct categories. In first two categories, NLC arises due to ferroelastic instabilities and correlated polyhedral rotations, respectively, which are often invoked in the description of other mechanical anomalies. Other two categories include materials having topological motifs that show predisposition towards NLC.

For example, third category consists of helical geometric motif which naturally occur in muscles as mechanism of muscular responses is governed by generating and exploiting NLC.[4] The NLC phenomenon reported in metals (Se[5] and Te[6]), supramolecular polymers,[7] and even in zeolite $AlPO_4$ single crystals[8] belongs to the helical motif category. Finally, forth category consists of wine-rack and honeycomb geometric motifs where the NLC is driven by the flexibility of the framework and extreme mechanical anisotropy. It is believed that such motifs can be considered in terms of flexible hinges and strong and inflexible struts.[9]

Only a handful of NLC materials have been discovered so far and many of them are inorganic.[1–3] A few organic and/or hybrid organic-inorganic materials show NLC phenomena and mostly belongs to the forth category of classification. For example, Fortes *et al.* have demonstrated that small molecule organic systems can adopt both NLC behavior and negative axial thermal expansion in the hydrogen-bonded "lattice fence" arrangement in methanol monohydrate, $(NH_4)_2C_2O_4.H_2O$, and 3-methyl-4-nitropyridine N-oxide.[10] The hinging-type lattice distortions under compression leading to NLC have been reported for metal-organic framework materials $[NH_4]Zn(HCOO)_3$,[11] [Ag(ethylenediamine)]NO_3,[12] MFM-133(M) (M=Zr,Hf),[13] Cu(4,4'-bpy)$_2$(H_2O)$_2$]·SiF_6[14] *etc.* A similar mechanism of NLC was revealed in topologically different structures of organometallic complexes [Fe(dipyrido[3,2-a:2'3'-c]phenazine)$_2$(NCS)$_2$].pyridine[15] and [(C_6F_5Au)$_2$(μ-1,4-diisocyanobenzene)].[16] Recently, 2D layered material Co(SCN)$_2$(pyrazine)$_2$ has also been reported to exhibit NLC with a layer sliding mechanism.[17]

In this study we use first-principles density functional theory (DFT) calculations i) to predict that $[NH_2NH_3][Co(HCOO)_3]$ can exhibit both positive and negative liner compressibility tunable by the pressure; (ii) to reveal the atomistic origin of the effect; (iii) to predict mechanical properties of this material.

All the electronic structure calculations are performed using a plane wave based Hubbard (U) corrected spin-polarized density functional theory (DFT+U) as implemented in Vienna Ab-initio Simulation package (VASP).[18,19] The electron-ion interactions are described by pro-

jector augmented wave (PAW) potential[20] and the Hubbard U correction is introduced using the method proposed by Dudarev *et al.*,[21] in which the U parameter (reflecting the strength of on-site Coulomb interaction) and J parameter (adjusting the strength of exchange interaction) are combined into a single parameter $U_{eff} = U\text{-}J$ to take care of the Coulomb repulsion between the localized d-electrons of Co. We use U_{eff}= 2.0 eV as proposed in previous studies.[22,23] Generalized gradient approximation (GGA) with Perdew-Burke-Ernzerhof (PBE) parameterization[24] is used for the exchange-correlation functional. The van der Waals interactions are incorporated within the GGA using zero-damping DFT-D3 method of Grimme *et al.*[25] We have previously found this computational approach provides good agreement for lattice parameters with experiment at zero pressure[26]. The most significant findings are cross-checked using different exchange correlation functional, Hubbard corrected local density approximation (LDA+U) in Ceperley-Alder (CA) parameterization,[27] and without dispersion corrections to ensure that findings are independent of the computational approach. A Monkhorst-Pack[28] k-space mesh of 5 × 5 × 3 in reciprocal space is used for the Brillouin zone integration and plane wave basis cutoff energy of 700 eV was used. The choices of k-mesh and cutoff energy provided energy convergence within 0.02 meV/atom. Full structural optimization was carried using conjugate gradient algorithm until the residual forces on ions were less than 0.002 eV/Å while the energy difference between two successive ionic optimization steps was less than 10^{-5} eV per supercell. Single crystal elastic constants are calculated using finite difference method[29] as implemented in the VASP package and further analyzed using ElAM software[30] in order to compute linear compressibilities, Young's moduli and Poisson ratios.

Experimentally, $[NH_2NH_3][Co(HCOO)_3]$ has been reported to undergo a structural phase transition from a nonpolar Pnma structure, with dynamical disorder in $NH_2NH_3^{+1}$ molecule, to a polar $Pna2_1$ structure below 343 K,[31] which was shown to be ferroelectric.[26] To obtain the ground state for this material we subject experimentally reported low temperature structure[31] to full structural relaxation. The ground state has $Pna2_1$ space group with structural

parameters reported in Ref[26] and G-type anti-ferromagnetic ordering of magnetic moments μ=2.69 μ_B on each Co^{2+} ion.[26] The calculated lattice parameters of 8.6, 7.7, 11.5 Å are in excellent agreement with experimental values of 8.7, 7.7, 11.5 Å reported at 100 K.[31]

Next, we apply hydrostatic pressure in the range of 0-6 GPa to the ground state and carry out full structural relaxation in the presence of pressure. Such simulations model application of hydrostatic pressure at low temperatures and were found to provide good agreement with experiment for TMCM-$MnCl_3$ and TMCM-$CdCl_3$ (TMCM = tri-methyl chloro-methyl ammonium).[32] We found no structural phase transitions in the given pressure range. Figure 1 reports pressure evolution of the supercell volume and lattice parameters. Fitting pressure-volume dependence to Birch–Murnaghan equation of state yields bulk modulus B_0 =27.9 GPa which is close to bulk moduli of 25.7-31.0 GPa measured for $[C(NH_2)_3]$-M-$(HCOO)_3$ (M=Cd,Co).[33,34] Figure 1(b) reveals that in the given pressure range the structure expands along the b-axis, that is the material exhibits NLC. We compute linear compressibilities along crystallographic axes (K_a, K_b, K_c) using the definition given in the introduction and reported the values in Table 1. In the same Table we provide values from the literature for materials in the same family. The comparison reveals (i) good agreement between our predictions and experimental measurements and (ii) a general trend among the materials: large anisotropy in compressibility along the three axes. In particular, they all exhibit high, intermediate, and low values of compressibility, with up to an order of magnitude difference between the values. The axis associated with the lowest value is likely to be prone to NLC. It is indeed believed that NLC materials possess high elastic anisotropy.[9]

Although our predictions for K_a, K_b, and K_c are in agreement with experimental findings from the literature (see Table 1 and Ref. Gao2020) it is important to test whether they are independent of the computational methodology adopted here. For that purpose we repeated some of the calculations using LDA exchange correlation functional with U_{eff} of 2.0 eV as described in the methodology. In agreement with GGA+U+D3 we found the LDA+U ground state to have G-AFM configuration. The LDA+U underestimated experimental zero pressure

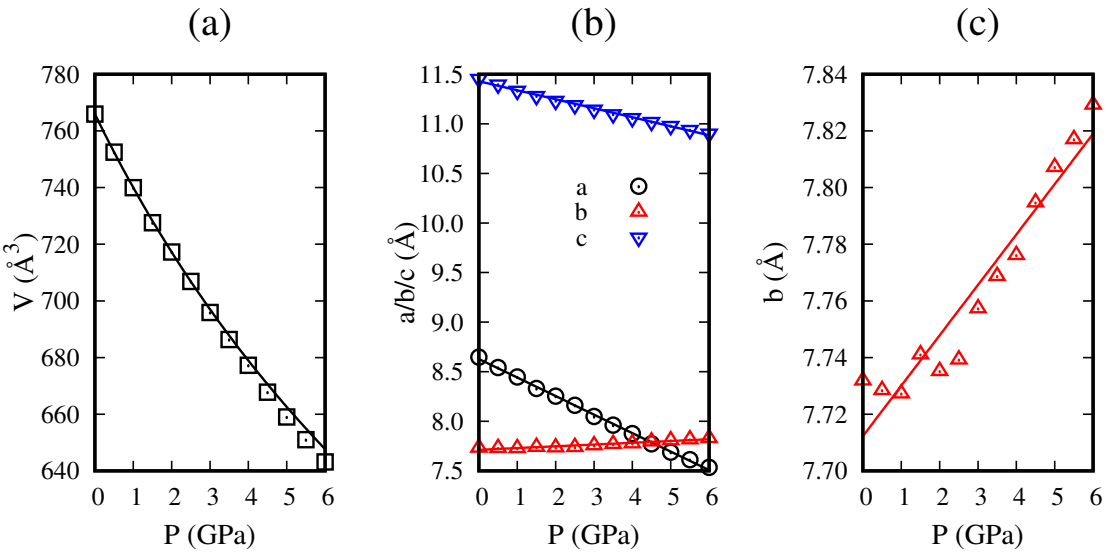

Figure 1: Dependence of the supercell volume, V, (a) and lattice parameters (b) and (c) on pressure, P. The solid lines give fit to Birch–Murnaghan equation of state in (a) and to linear dependence in (b) and (c).

lattice parameters by up to 4.5%. The bulk modulus computed by fitting volume-pressure data by the third order Birch–Murnaghan equation of state yielded 31.2 GPa which is 12% higher compared to our GGA+U+D3 calculated value but still in line with experimental values on other formate family member.[33,34] Most importantly, the LDA+U calculations also predict NLC along b-axes with the value of K_b=-1.9 TPa^{-1}, which demonstrates that our predictions are independent of computational methodology adopted in the present study.

Table 1: Linear compressibility of the lattice parameters (K_a, K_b, K_c), struts ($K_{r_{ab}}$) and hinges (K_θ) in TPa^{-1} of $[NH_2NH_3][Co(HCOO)_3]$ compared with experimental values of other materials in the same family.

system	Pressure range (GPa)	K_a	K_b	K_c	$K_{r_{ab}}$	K_{r_c}	K_θ
NH_2NH_3-$Co(HCOO)_3$	0.00-6.00	21.6	-2.3	7.9	9.2	6.8	-15.2
$C(NH_2)_3$-$Mn(HCOO)_3$	0.00-1.12[33]	26.6	15.4	0.11	16.2	12.4	17.7
$C(NH_2)_3$-$Co(HCOO)_3$	0.00-1.19[33]	20.7	12.5	0.96	11.4	10.1	13.2
$C(NH_2)_3$-$Zn(HCOO)_3$	0.00-0.66[35]	18.3	3.6	8.4			
$C(NH_2)_3$-$Cu(HCOO)_3$	0.00-0.66[35]	28.7	4.0	11.9			
NH_4-$Zn(HCOO)_3$	0.00-1.00[11]	15.8	-	-1.8			

Furthermore, we investigated whether NLC occurs for other types of magnetic ordering (A-, and C-type antiferromagnetism and ferromagnetism) and found that the effect persists for all orderings considered.

To elucidate the origin of NLC in this material we turn to the maps of Young's moduli, E, given in Fig. 2. The maps demonstrate high anisotropy in mechanical response of the material with [001] being the hardest direction followed by [110] direction. Figure 3(a) reveals that these are the directions of CoO_6 chains and formate ligands, respectively. It also shows that the structure belongs to the wine-rack type[2] that is capable of exhibiting negative compressibility via strut-hinge mechanism.[33] In Fig. 3(a) the struts and hinges are denoted with r_{ab} and Θ, respectively. In such mechanism the hinge angle increase under pressure could overtake strut deformation and give origin to NLC as depicted in Fig. 3(e). The mechanism is believed to be activated when intrinsic rigidity of molecular moieties overpowers intermolecular hinges.[33] To test whether the model can explain our findings we compute r_{ab} and Θ as a function of pressure and plot them in Fig. 3(c). Indeed, we find significant increase in the hinge angle. The strut length decreases under compression. We used linear fit to the computational data to obtain linear compressibilities for the hinges and struts, K_θ and $K_{r_{ab}}$, respectively, which are reported in Table 1. The data reveal that $|K_\theta| = 1.7K_{r_{ab}}$ which confirms that the increase in the hinge angle is indeed the origin of NLC in this material.

To ensure that these findings are the result of molecular blocks rigidity, we computed their bond lengths and bond angles as a function of pressure. In the formate ligand, we found almost no change in the C-O bond length or O-C-O bond angles which reflects the rigidity of the ligand due to strong covalent bonding. In the CoO_6 unit we find up to 2.5% decrease in the Co-O bond. We conclude that the individual units are indeed rigid under pressure. Recall that it is along the directions of these units the structure exhibits strongest mechanical response (see Fig. 2(a)). The alternative mechanism for pressure accommodation is tilting of the units. The oxygen octahedra tilts can be quantified by the dihedral angles indicated

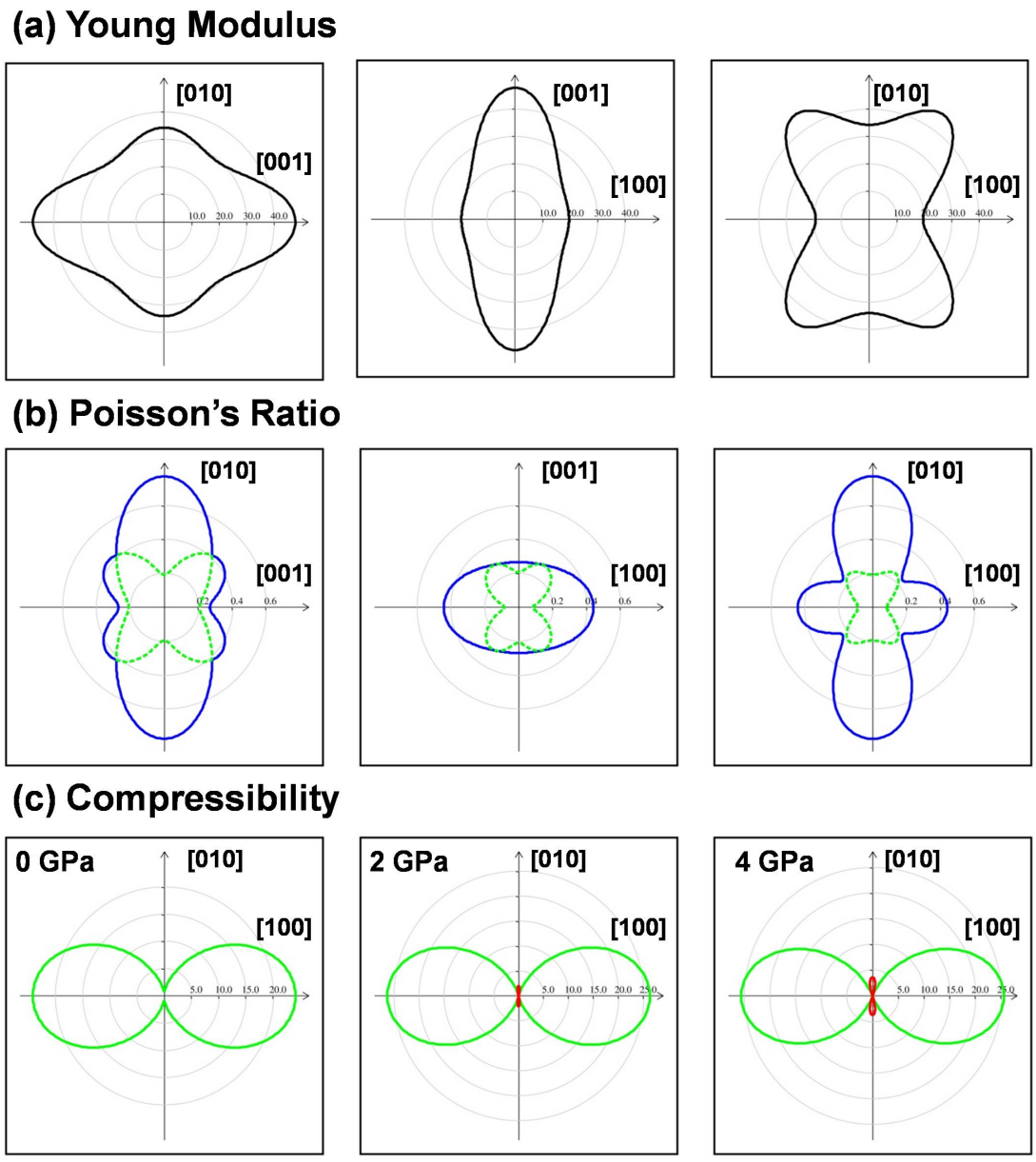

Figure 2: The 2D plots of Young's moduli (a), and Poisson ratios (b) at zero pressures; and linear compressibilities at 0 GPa, 2 GPa, and 4 GPa pressures (c). In (b) the blue outer line and green inner line show the maximum and minimum values, respectively. In (c) green line show the maximum values and red line shows negative values.

in Fig. 3(b) and (d). Pressure evolution of these angles is given in Fig. 3(d) and reveals that significant tilts (up to 26%) indeed take place to accommodate pressure. In particular,

the change in the tilt angle O_1-Co_1-Co_2-O_2 causes the change in the Co-O-C angle by 7° which causes r to decrease while Θ increase at the same time. Thus, our structural analysis supports the strut-hinge model originating from tilting of relatively rigid structural units (formates, and oxygen octahedra).

Materials with NLC are also known to exhibit other anomalous properties such as anomalous Poisson ratios. The map of Poisson ratios is given in Fig. 2(b) and reveals extreme anisotropy in materials response to uniaxial deformation. For example, deformation along [010] direction yields 0.19 and 0.77 as minimum and maximum values for Poisson ratio, respectively. Similarly, deformation along [100] direction produces largely different minimum and maximum values of the Poisson ratio.

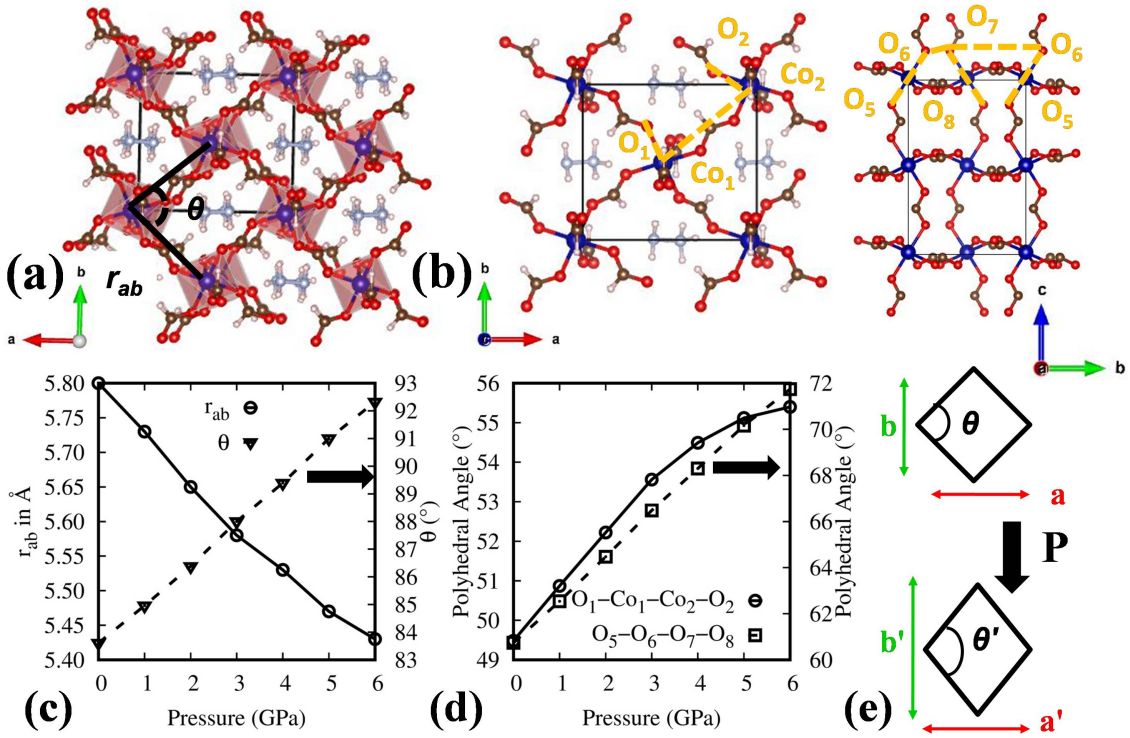

Figure 3: (a) Structure of $[NH_2NH_3][Co(HCOO)_3]$ shown in different planes to indicate angles and distances (a)-(b). Color scheme: Co^{2+}, blue; O, red; C, brown; H, gray. Dependence of strut length and hinge angle (c) and diherdal angles (d) on pressure. Schematics of the negative compressibility due to hinge-strut model (e).

Next we set to find out whether negative compressibility effect exhibits pressure depen-

Table 2: Single crystal elastic constants C_{ij} (in GPa) and linear compressibilities K (in TPa^{-1}) along crystallographic axes computed at different pressures.

	C_{11}	C_{12}	C_{13}	C_{22}	C_{23}	C_{33}	C_{44}	C_{55}	C_{66}	$K(100)$	$K(010)$	$K(001)$
0 GPa	33.8	29.7	15.3	62.3	23.3	57.6	9.7	8.8	16.8	24.4	0.4	11.0
2 GPa	34.0	33.1	19.7	68.5	30.7	62.3	8.9	11.3	15.7	26.5	-2.1	8.6
4 GPa	37.5	39.6	23.0	85.1	37.2	68.3	9.9	15.1	13.3	25.6	-3.7	7.8

dence. For that we compute linear compressibility at different pressures using the equation $K_i = \sum_{j=1}^{3} S_{iijj}$, where S_{iijj} are the components of elastic compliance tensor computed at different pressures, and i and j denote principal axes. Technically, fully relaxed structures at pressures 0, 2 and 4 GPa are used to compute elastics constants at those pressures which are reported in Table 2. The constants are then used in ElAM software[30] to obtain K_i reported in the same Table and plotted in Fig 2(c). Surprisingly, the calculations predict that at zero pressure the material does not exhibit NLC and that the effect onsets as the pressure increases. At 2 GPa the material displays NLC of -2.1 TPa^{-1} which further decreases to -3.7 TPa^{-1} at 4 GPa pressure. Thus, we find that pressure has stabilizing effect on the NLC that is also evident from Fig 2(c). To look into this change of sign further we replot the dependence of b lattice parameter on pressure in Fig. 1(c). Indeed we find that below 1 GPa the lattice parameter decreases as a function of pressure providing direct confirmation of positive linear compressiblity in the limit of low pressures. Above 1 GPa the coefficient changes sign. Similar behavior has been reported in $Zn(HO_3PC_4H_8PO_3H)\cdot 2H_2O$ (ZAG-4) metal-organic framework where both positive (in 0-2 GPa range) and negative (at higher pressures) linear compressibility is observed along b-crystallographic direction.[36] Small fluctuations in the c-lattice parameters in Fig. 1 panel (c) are due to the chosen convergence criteria. A few points in the graph have been recalculated using energy convergence criteria of 10^{-8} eV and 10^{-7} eV, for two successive electronic self-consistent steps and ionic optimization steps, respectively. The fluctuations went away, while the dependence remained the same. Interestingly, the zero pressure coefficients are in excellent agreement with experimental data for $C(NH_2)_3$-$X(HCOO)_3$ (X = Mn, Co, Zn, Cu) reported in Table 1 which

suggests that these materials may also exhibit NLC under higher pressure.

In summary, we used first-principles DFT simulations to predict that hybrid organic inorganic ferroelectric perovskite, $[NH_2NH_3][Co(HCOO)_3]$, can exhibit both positive and negative linear comrpessibility under hydrostatic pressure. In the zero pressure limit all three compressibility values (K_a, K_b and K_c) are positive. The noteworthy feature is extremely small value of compressibility along b crystallographic direction. As pressure increases this value changes its sign into negative and continue to decrease as pressure increases. In other words, pressure stabilizes NLC in this material. Comparison of our findings with experimental results from the literature for similar materials reveal that they all exhibit large anisotropy of K_a, K_b and K_c with one of the values being exceptionally small. This observation suggest that our predictions may be applicable to a a wider range of materials. Detailed structural investigation confirmed that the NLC in $[NH_2NH_3][Co(HCOO)_3]$ originates from the tilting of relatively rigid molecular units (CoO_6 polyhedra and $HCOO^{-1}$ ligands) whose "hinge" angle in the "wine-rack" geometry increases under pressure. Mechanical properties are highly anisotropic. We believe that our study advances understanding of this versatile class of materials and will promote further research in this area.

The work is supported by the National Science Foundation under the grant EPMD-2029800.

References

(1) Baughman, R. H.; Stafström, S.; Cui, C.; Dantas, S. O. Materials with Negative Compressibilities in One or More Dimensions. *Science* **1998**, *279*, 1522–1524.

(2) Cairns, A. B.; Goodwin, A. L. Negative linear compressibility. *Phys. Chem. Chem. Phys.* **2015**, *17*, 20449–20465.

(3) Goodwin, A. L.; Keen, D. A.; Tucker, M. G. Large negative linear compressibility of

$Ag_3[Co(CN)_6]$. *Proceedings of the National Academy of Sciences* **2008**, *105*, 18708–18713.

(4) Kier, W. M.; Smith, K. K. Tongues, tentacles and trunks: the biomechanics of movement in muscular-hydrostats. *Zoological Journal of the Linnean Society* **2008**, *83*, 307–324.

(5) McCann, D. R.; Cartz, L.; Schmunk, R. E.; Harker, Y. D. Compressibility of Hexagonal Selenium by X-Ray and Neutron Diffraction. *Journal of Applied Physics* **1972**, *43*, 1432–1436.

(6) Keller, R.; Holzapfel, W. B.; Schulz, H. Effect of pressure on the atom positions in Se and Te. *Phys. Rev. B* **1977**, *16*, 4404–4412.

(7) Paliwoda, D.; Wawrzyniak, P.; Katrusiak, A. Unwinding $Au^+\cdots Au^+$ Bonded Filaments in Ligand-Supported Gold(I) Polymer under Pressure. *The Journal of Physical Chemistry Letters* **2014**, *5*, 2182–2188.

(8) Ren, W.; Ye, J.-T.; Shi, W.; Tang, Z.-K.; Chan, C. T.; Sheng, P. Negative compressibility of selenium chains confined in the channels of $AlPO_4$-5 single crystals. *New Journal of Physics* **2009**, *11*, 103014.

(9) Ogborn, J. M.; Collings, I. E.; Moggach, S. A.; Thompson, A. L.; Goodwin, A. L. Supramolecular mechanics in a metal-organic framework. *Chem. Sci.* **2012**, *3*, 3011–3017.

(10) Fortes, A. D.; Suard, E.; Knight, K. S. Negative Linear Compressibility and Massive Anisotropic Thermal Expansion in Methanol Monohydrate. *Science* **2011**, *331*, 742–746.

(11) Li, W.; Probert, M. R.; Kosa, M.; Bennett, T. D.; Thirumurugan, A.; Burwood, R. P.; Parinello, M.; Howard, J. A. K.; Cheetham, A. K. Negative Linear Compressibility of

a Metal-Organic Framework. *Journal of the American Chemical Society* **2012**, *134*, 11940–11943.

(12) Cai, W.; Katrusiak, A. Giant negative linear compression positively coupled to massive thermal expansion in a metal-organic framework. *Nature Communications* **2014**, *5*, 4337.

(13) Yan, Y.; O'Connor, A. E.; Kanthasamy, G.; Atkinson, G.; Allan, D. R.; Blake, A. J.; Schroder, M. Unusual and Tunable Negative Linear Compressibility in the Metal-Organic Framework MFM-133(M) (M = Zr, Hf). *Journal of the American Chemical Society* **2018**, *140*, 3952–3958.

(14) Chen, Z.; Xu, B.; Li, Q.; Meng, Y.; Quan, Z.; Zou, B. Selected Negative Linear Compressibilities in the Metal-Organic Framework of $[Cu(4,4'\text{-bpy})_2(H_2O)_2]\cdot SiF_6$. *Inorganic Chemistry* **2020**, *59*, 1715–1722.

(15) Shepherd, H. J.; Palamarciuc, T.; Rosa, P.; Guionneau, P.; Molnar, G.; Letard, J.-F.; Bousseksou, A. Antagonism between Extreme Negative Linear Compression and Spin Crossover in $[Fe(dpp)_2(NCS)_2]$.py. *Angewandte Chemie International Edition* **2012**, *51*, 3910–3914.

(16) Woodall, C. H.; Beavers, C. M.; Christensen, J.; Hatcher, L. E.; Intissar, M.; Parlett, A.; Teat, S. J.; Reber, C.; Raithby, P. R. Hingeless Negative Linear Compression in the Mechanochromic Gold Complex $[(C_6F_5Au)_2(\mu\text{-}1,4\text{-diisocyanobenzene})]$. *Angewandte Chemie International Edition* **2013**, *52*, 9691–9694.

(17) Zeng, Q.; Wang, K.; Qiao, Y.; Li, X.; Zou, B. Negative Linear Compressibility Due to Layer Sliding in a Layered Metal-Organic Framework. *The Journal of Physical Chemistry Letters* **2017**, *8*, 1436–1441.

(18) Kresse, G.; Hafner, J. Ab initio molecular dynamics for liquid metals. *Phys. Rev. B* **1993**, *47*, 558–561.

(19) Kresse, G.; Furthmuller, J. Efficiency of ab-initio total energy calculations for metals and semiconductors using a plane-wave basis set. *Computational Materials Science* **1996**, *6*, 15 – 50.

(20) Blöchl, P. E. Projector Augmented-Wave Method. *Phys. Rev. B: Condens. Matter Mater. Phys.* **1994**, *50*, 17953–17979.

(21) Dudarev, S.; Botton, G.; Savrasov, S.; Humphreys, C.; Sutton, A. Electron-energy-loss spectra and the structural stability of nickel oxide:An LSDA+U study. *Phys. Rev. B* **1998**, *57*, 1505.

(22) Fung, V.; Tao, F. F.; en Jiang, D. Trends of Alkane Activation on Doped Cobalt (II, III) Oxide from First Principles. *ChemCatChem* **2018**, *10*, 244–249.

(23) Liu, J.; Zhang, S.; Zhou, Y.; Fung, V.; Nguyen, L.; Jiang, D.; Shen, W.; Fan, J.; Tao, F. F. Tuning catalytic selectivity of oxidative catalysis through deposition of non-metallic atoms in surface lattice of metal oxide. *ACS Catal.* **2016**, *6*, 4218–4228.

(24) Perdew, J. P.; Burke, K.; Ernzerhof, M. Generalized Gradient Approximation Made Simple. *Phys. Rev. Lett.* **1996**, *77*, 3865–3868.

(25) Grimme, S.; Antony, J.; Ehrlich, S.; Krieg, H. A consistent and accurate ab initio parametrization of density functional dispersion correction (DFT-D) for the 94 elements H-Pu. *J. Chem. Phys.* **2010**, *132*, 154104.

(26) Ghosh, P.; DeTellem, D.; Ren, J.; Witanachchi, S.; Ma, S.; Lisenkov, S.; Ponomareva, I. unpublished.

(27) Ceperley, D. M.; Alder, B. J. Ground State of the Electron Gas by a Stochastic Method. *Phys. Rev. Lett.* **1980**, *45*, 566–569.

(28) Monkhorst, H. J.; Pack, J. D. Special points for Brillouin-zone integrations. *Phys. Rev. B: Condens. Mater. Phys.* **1976**, *13*, 5188.

(29) Page, Y. L.; Saxe, P. Symmetry-general least-squares extraction of elastic data for strained materials from ab initio calculations of stress. *Phys. Rev. B* **2002**, *65*, 104104.

(30) Marmier, A.; Lethbridge, Z. A.; Walton, R. I.; Smith, C. W.; Parker, S. C.; Evans, K. E. ElAM: A computer program for the analysis and representation of anisotropic elastic properties. *Computer Physics Communications* **2010**, *181*, 2102–2115.

(31) Gunatilleke, W. D. C. B.; Wei, K.; Niu, Z.; Wojtas, L.; Nolas, G.; Ma, S. Thermal conductivity of a perovskite-type metal-organic framework crystal. *Dalton Trans.* **2017**, *46*, 13342–13344.

(32) Ghosh, P. S.; Doherty, J.; Lisenkov, S.; Ponomareva, I. Tunability of Structure, Polarization, and Band Gap of High T_c Organic-Inorganic Ferroelectrics by Hydrostatic Pressure: First-Principles Study. *The Journal of Physical Chemistry C* **2021**, *125*, 16296–16303.

(33) Viswanathan, M. Structural Tunability Controlled by Uniaxial Strength in a Hybrid Perovskite. *The Journal of Physical Chemistry C* **2019**, *123*, 6711–6716.

(34) Yang, Z.; Cai, G.; Bull, C. L.; Tucker, M. G.; Dove, M. T.; Friedrich, A.; Phillips, A. E. Hydrogen-bond-mediated structural variation of metal guanidinium formate hybrid perovskites under pressure. *Philosophical Transactions of the Royal Society A: Mathematical, Physical and Engineering Sciences* **2019**, *377*, 20180227.

(35) Gui, D.; Ji, L.; Muhammad, A.; Li, W.; Cai, W.; Li, Y.; Li, X.; Wu, X.; Lu, P. Jahn-Teller Effect on Framework Flexibility of Hybrid Organic-Inorganic Perovskites. *The Journal of Physical Chemistry Letters* **2018**, *9*, 751–755.

(36) Gagnon, K. J.; Beavers, C. M.; Clearfield, A. MOFs Under Pressure: The Reversible Compression of a Single Crystal. *Journal of the American Chemical Society* **2013**, *135*, 1252–1255.